Research Article | Vol. 11, No. 9 / 1 September 2020 / Biomedical Optics Express 4890
Biomedical Optics EXPRESS

Moxifloxacin based axially swept wide-field fluorescence microscopy for high-speed imaging of conjunctival goblet cells

JUNGBIN LEE,[1,5] SEONGHAN KIM,[1,5] CHANG HO YOON,[2,3] MYOUNG JOON KIM,[4] AND KI HEAN KIM[1,*]

[1]Department of Mechanical Engineering, Pohang University of Science and Technology, 77 Cheongam-Ro, Nam-gu, Pohang, Gyeongbuk 37673, South Korea
[2]Department of Ophthalmology, Seoul National University College of Medicine, 103 Daehak-ro, Jongno-gu, Seoul 03080, South Korea
[3]Laboratory of Ocular Regenerative Medicine and Immunology, Seoul Artificial Eye Center, Seoul National University Hospital Biomedical Research Institute, 101 Daehak-ro, Jongno-gu, Seoul 03080, South Korea
[4]Renew Seoul Eye Center, 528 Teheran-ro, Gangnam-gu, Seoul 06181, South Korea
[5]These authors contributed equally
*kiheankim@postech.ac.kr

Abstract: Goblet cells (GCs) in the conjunctiva are specialized epithelial cells producing mucins on the ocular surface. GCs play important roles in maintaining homeostasis of the ocular surface, and GC dysfunction is associated with various complications including dry eye diseases. Current GC examination methods, which are conjunctival impression cytology and confocal reflection microscopy, have limitations for routine examination. Fluorescence microscopy using moxifloxacin was recently introduced as a non-invasive and high-contrast imaging method, but further development is needed to be used for GC examination. Here we developed a non-invasive high-speed high-contrast GC imaging method, called moxifloxacin based axially swept wide-field fluorescence microscopy (MBAS-WFFM). This method acquired multiple fluorescence images with the axial sweeping of the focal plane to capture moxifloxacin labeled GCs on the tilted conjunctival surface in focus and generated all-in-focus images by combining the acquired images. The imaging field of view and imaging speed were increased to 1.6 mm × 1.6 mm and 30 fps. An image processing method was developed for the analysis of GC density. MBAS-WFFM was applied to alkali burn mouse models and detected GC damage and recovery via longitudinal imaging. MBAS-WFFM could assess the status of GCs rapidly and non-invasively. We anticipate MBAS-WFFM to be a starting point for non-invasive GC examination and the diagnosis of GC associated diseases. For example, MBAS-WFFM could be used to classify dry eye diseases into detail categories for effective treatment.

1. Introduction

Conjunctival goblet cells (GCs) are specialized epithelial cells in the conjunctiva, secreting mucins on the ocular surface [1,2]. Mucins together with waters and lipids constitute tear film, which is important for the ocular surface protection [2,3]. Mucins lubricate the ocular surface to maintain the wet environment. GC dysfunction is associated with various ocular diseases including dry eye disease, Sjögren syndrome, graft versus host disease (GVHD) [4–8]. The roles of GCs in the conjunctiva were understood further with the recent development of *Spdef* null mice which do not have GCs in the conjunctiva [9]. Without GCs, there was the increase of corneal surface damage and tear volume. Epithelial cells in the conjunctiva expressed high levels of stress genes, and there was the increase of inflammatory cells in the conjunctiva. Therefore, GCs are important for the homeostasis of the ocular surface. Also, GCs are an important indicator

#401896 https://doi.org/10.1364/BOE.401896
Journal © 2020 Received 6 Jul 2020; revised 29 Jul 2020; accepted 29 Jul 2020; published 6 Aug 2020

Biomedical Optics EXPRESS

in the prognosis of alkali burn [10–12]. Therefore, the examination method of GCs is important for the diagnosis and treatment monitoring of various ocular surface complications.

The GC examination methods, currently available in the clinic, are conjunctival impression cytology (CIC) and reflectance confocal microscopy (RCM) [13,14]. CIC extracts cells on the surface of conjunctiva including GCs by using a filter paper, and then the density of GCs is analyzed via the microscopic examination of the extracted cells with Periodic acid-Schiff (PAS) staining [15]. Although CIC is useful for cellular examination and biomarker investigation on the ocular surface, it can cause discomfort and irritation in some patients [16]. Additionally, the CIC protocol is not standardized [17,18]. RCM is a non-invasive imaging method based on light reflection, and visualized GCs as hyper-reflective large round cells compared to other epithelial cells [19]. Although RCM has potential as the GC examination method, RCM examination requires clinicians some training for the analysis of RCM images due to relatively low image contrast and a relatively small imaging field of view (FOV) of a few hundred micrometers [20,21]. Therefore, the current methods have limitations for routine GC examination. Non-invasive and fast GC examination methods will be useful for the diagnosis of ocular surface diseases [22,23]. With moxifloxacin labeling, 3D fluorescence microscopy techniques such as confocal fluorescence microscopy (CFM) and two-photon microscopy (TPM) could visualize GCs in high contrasts in mouse models, *in vivo* [23]. Fluorescence imaging methods using moxifloxacin for GC labeling can be clinically compatible by using the FDA approved drug. However, moxifloxacin-based 3D fluorescence microscopy had several limitations for the GC examination in the imaging speed, imaging FOV, and complexity. The imaging speed was limited due to the sequential point-wise scanning of specimens, and the imaging speed of up to 7 fps was demonstrated previously. 3D fluorescence microscopy had small FOVs by using high-magnification objective lenses for high-resolution imaging. 3D fluorescence microscopies are complex and expensive to be used in the clinic. In order to overcome the limitations of 3D fluorescence microscopy, wide-field fluorescence microscopy (WFFM) was tested for GC imaging. WFFM could image GCs on the surface of conjunctiva at the higher imaging speed (30 fps) and in the larger FOV than those of 3D fluorescence microscopy. However, WFFM could not capture all the GCs in the conjunctiva in focus due to the tilt and irregularity of the conjunctival surface and its limited depth of field (DOF).

In this study, we developed moxifloxacin based axially swept WFFM (MBAS-WFFM) for the in-focus imaging of all the GCs. The system was designed to take multiple WFFM images with the axial sweeping of the focal plane. The acquired WFFM images were processed to generate all-in-focus images. An image processing algorithm was developed to analyze GC density. The new GC imaging system was characterized in normal mice and applied to alkali burn mouse models for testing the ability of detecting GC damage and recovery.

2. Methods

2.1. MBAS-WFFM system

A simple schematic of MBAS-WFFM and a series of WFFM images acquired with the axial sweeping are shown in Fig. 1. The MBAS-WFFM system was based on WFFM configuration. A 405nm light emitting diode (M405L3, Thorlabs) was used as the excitation light source. Excitation light from the source was transmitted through an excitation filter (ZET405/20x, Chroma), reflected on a dichroic mirror (T425lpxr, Chroma) toward an objective lens (Plan N, 10X, 0.25NA, Olympus). The objective lens illuminated excitation light onto the specimen uniformly. Emission light generated from the specimen was collected back by the objective lens, transmitted through the dichroic mirror and an emission filter (ET430lp, Chroma), and focused on a sCMOS camera (pco.edge 4.2, PCO). The objective lens was mounted on a motorized translational stage (Z825B, Thorlabs) for the axial translation of the focal plane. The objective lens was an air type lens with 10 mm working distance so that the specimen could be imaged

Biomedical Optics EXPRESS

without any physical contact. The imaging field of view (FOV) was 1.6 mm × 1.6 mm, and the image resolution was 1.3 μm, limited by the camera. The imaging speed was 30 frames/s, which was limited by the camera speed. The WFFM system had a shallow DOF of approximately 30 μm. The specimen to be imaged was the conjunctiva of live mouse models so that the surface of specimen could be tilted with respect to the focal plane of the imaging system. Therefore, the conjunctival surface in FOV could not be captured in focus owing to the shallow DOF. In order to image GCs in the tilted conjunctiva in focus, multiple WFFM images were acquired with the axial translation of the focal plane. The acquired multiple WFFM images were processed to generate single all-in-focus images. The objective lens was initially positioned to have the focal plane at the deepest location of the specimen surface. Then, the focal plane was swept outward by the translation of the objective lens with continuous WFFM imaging. The typical range of axial translation was approximately a few millimeters and the total imaging time was less than 2s. The power of excitation light onto the specimen was approximately 0.21 mW and the total excitation energy used in the imaging was approximately 0.2 J/cm^2. This excitation energy level was approximately 100 times lower than the reported damage threshold (54 J/cm^2) [24].

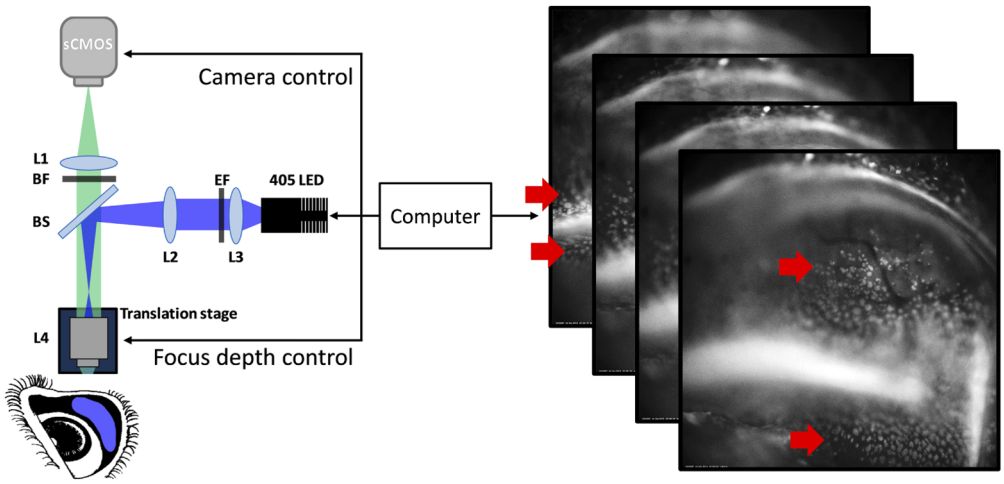

Fig. 1. A schematic of MBAS-WFFM system and a stack of axially swept WFFM images. L1: achromatic lens (f = 150 mm), L2: achromatic lens (f = 150 mm), L3: achromatic lens (f = 50 mm), L4: objective lens, EF: excitation filter, BS: dichroic mirror, BF: emission filter. Red arrows indicate in-focus areas in the WFFM images.

2.2. *Image processing algorithms*

Multiple partially focused WFFM images, acquired with the axial sweeping of the focal plane, were processed first to generate a single all-in-focus image. Then quantitative information of GCs such as GC density was analyzed by another processing procedure. A flow chart showing the image processing procedure is shown in Fig. 2. For the merging of the axially swept WFFM images into the all-in-focus image, an open-source image stacking algorithm (FSTACK algorithm, Joe Yeh, MIT license) was adapted. Briefly, the FSTACK algorithm utilized the Laplacian of Gaussian (LoG) filter to detect the edges of objects such as GCs with zero-crossing in all stacked images. The focal planes, which have the largest LoG responses in all the stacked images, were found. Then, the focal planes were combined to form the all-in-focus image. The performance of the FSTACK algorithm in combining axially swept WFFM images was verified by imaging a depth-of-field target (DOF 5-15, Edmund Optics GmbH, Karlsruhe, Germany) as the specimen. Quantitative analysis of GCs was conducted in the all-in-focus WFFM image. A region of

Biomedical Optics EXPRESS

interest (ROI) was selected in the image, and the one selected in Fig. 2(c) as an example was approximately 340 μm × 340 μm in size. The ROI was processed in the following steps: (1) noise reduction by using the bilateral filter with edge preservation [25], (2) contrast enhancement and equalization by using the contrast-limited adaptive histogram equalization method (Fig. 2(d)) [26], (3) thresholding by using the 'sobel' edge detection algorithm [27], and conversion to a binary image (Fig. 2(e)). The binary ROI image was processed to obtain GC density. The density was calculated by dividing the total area of GCs with both a single GC size and the area of ROI in the binary image (Fig. 2(f)). The size of individual GCs in the mouse conjunctiva was measured by using the MBAS-WFFM images of *ex-vivo* normal mouse conjunctiva specimens (Supplement 1). Approximately 10 isolated GCs in the images were analyzed, and their size was 12 ± 4 μm in diameter on average. The measurement result was consistent with the previous report which showed the GC size to be 11 μm in diameter [28]. All the image processing procedures were conducted in MATLAB (Matlab 2018a, Mathworks). The processing time for generating an all-in-focus image was less than 5s by using GPU.

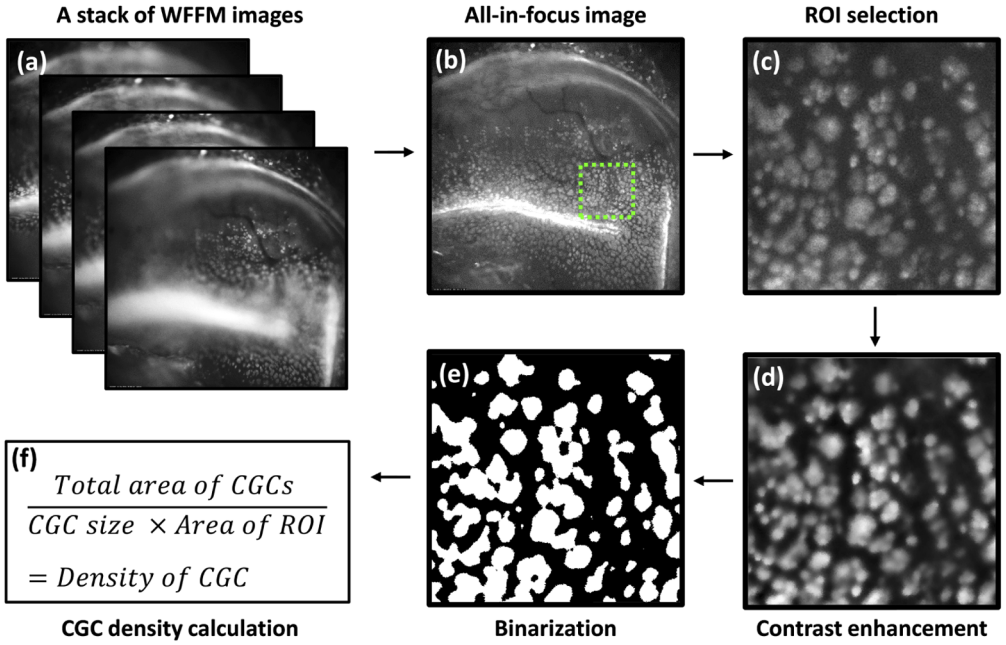

Fig. 2. Image processing flowchart. (a) a stack of axially swept WFFM images, (b) an all-in-focus image reconstructed by using an image stacking algorithm (FSTACK), (c) a magnified image from the selected region of interest (ROI) in the all-in-focus image, (d) a contrast enhanced image by using bilateral filter and contrast-limited adaptive histogram equalization, (e) a binary image, (f) a formula for GC density calculation.

2.3. Mouse model preparation and the imaging protocol

Seven 8-week-old SKH1-Hrhr male mice were used for *in-vivo* GC imaging experiment. All the animal experimental procedures were approved by the Institutional Animal Care & Use Committee at the Pohang University of Science and Technology (IACUC, approval number: POSTECH- 2015-0030-R2) and were conducted in accordance with the guidelines. Five mice were used as the alkali burn models, and the other two mice were used as the control models. The alkali burn models and control models were imaged longitudinally: before and right after the burn induction, and then every 5 days afterwards until 30 days. Two alkali burn models were

Biomedical Optics EXPRESS

euthanized via anesthetized manual cervical dislocation for histology during the longitudinal imaging: one right after the burn induction and the other on day 30 post-burn. One control model was sacrificed for histology in the same way. Before both the imaging and alkali burn induction, mice were anesthetized by using a face mask administering a gas mixture of 1.5%/vol. isoflurane (Terrel TM, Piramal) and medical-grade oxygen, and held by using a custom mouse eye holder consisting of a stereotactic device with ear bars. Alkali burn was induced in one eye according to the protocol in the previous literature [12]. In brief, a small piece of wipe tissue (KIMTECH, 1 mm × 1 mm in size) soaked in 0.5M NaOH solution was placed onto the conjunctiva for 30 s while the eyelid of the mouse eye was left open. Then, the burned eye was washed with 10 ml phosphate-buffered saline (PBS) solution. Moxifloxacin ophthalmic solution (Vigamox, Alcon Laboratories, Fort Worth, USA) was used as a labeling agent. Drops of moxifloxacin ophthalmic solution were instilled onto the eye and incubated for 3 minutes with the eyelid closed. During the imaging, the eyelid was rolled open and fixed with taping. Both the MBAS-WFFM images and bright-field images were acquired.

3. Results

3.1. MBAS-WFFM imaging and GC analysis in normal mouse models, in vivo

The new GC imaging system was characterized by imaging the conjunctiva in normal mice, *in vivo*. The imaging results are shown in Fig. 3. A single WFFM image at a single focal plane, all-in-focus WFFM images of GCs in 2 different FOVs, and a corresponding bright-field image in the same region are shown in Figs. 3(a)–3(c), respectively. The single WFFM image showed partially focused GCs in the conjunctiva due to the tilted and non-flat conjunctival surface. GCs were in focus in two regions of the image, marked with red dashed lines, and out of focus in the other regions. The generated all-in-focus WFFM images showed all the GCs in the FOV in focus (Fig. 3(b)). The overall distribution of GCs and GC clusters was seen in the full FOV image, but individual GCs were too small to be resolved. A boxed region in the full FOV image was magnified to resolve individual GCs (Fig. 3(b1)). The magnified image showed GC clusters in various sizes and some isolated GCs. The full FOV image captured part of the conjunctiva. A band structure with strong fluorescence in the middle of the image was the folded zone of the conjunctiva with remaining moxifloxacin ophthalmic solution. GC density was the highest around the folded region and decreased gradually away from the folded region on both sides. The spatial variation of GC density was consistent with the previous report [29]. The WFFM images showed blood vessels in the conjunctiva in negative contrasts owing to the strong absorption of both excitation and emission light. Blood vessels were visualized in the bright-field image as well so that the vessels could be used as landmarks for the spatial co-registration of the images acquired at different time points.

3.2. Longitudinal observation of GC distribution in alkali burn mouse models

After the demonstration and characterization in the normal mouse models, MBAS-WFFM was applied to the alkali burn mouse models to observe GC damage and recovery. GC imaging was performed longitudinally, once before the burn induction as the reference and then several times periodically after the burn induction. The imaging results with PAS histology are shown in Fig. 4. Representative WFFM GC images of a mouse model before, right after, and in 30 days after the burn induction are presented. WFFM images in the full FOV and magnified images from the green boxed regions of the full FOV images are presented to show both the gross GC distributions and the individual GCs or GC clusters. The magnified images at different time points showed almost the same conjunctival region, although blood vessels in the images were dissimilar due to the alkali burn and the regeneration afterward. Before the alkali burn, the WFFM images showed dense GCs and GC clusters in the mouse conjunctiva. GCs in the conjunctiva were

Biomedical Optics EXPRESS

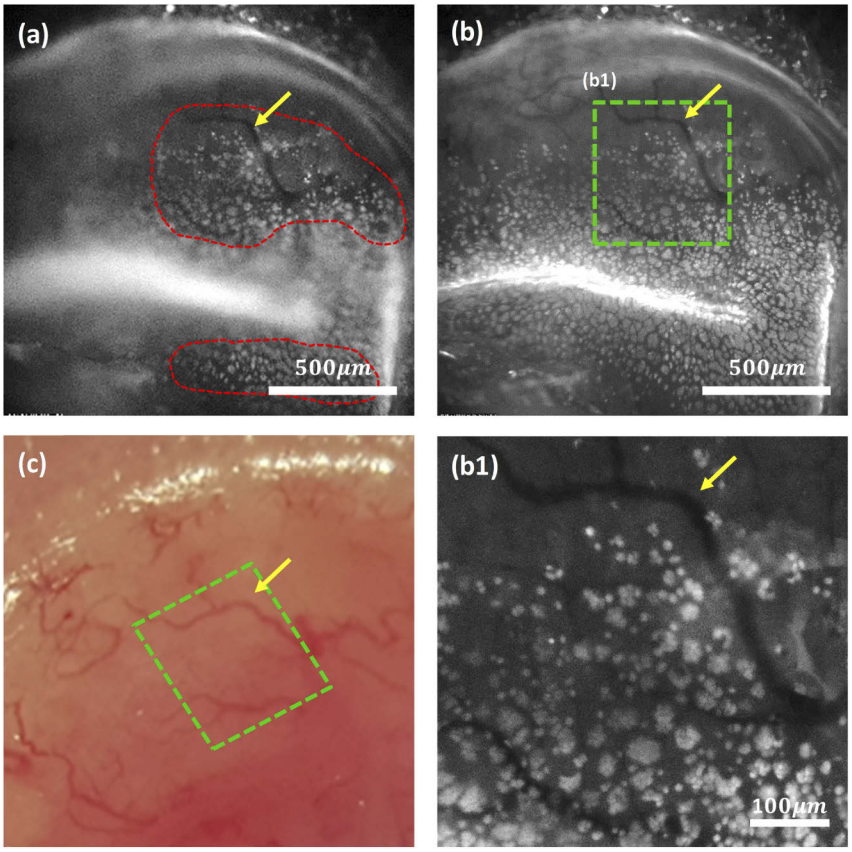

Fig. 3. MBAS-WFFM images and a bright-field image of the normal mouse conjunctiva, *in vivo*. (a) A single-plane WFFM image, (b) an all-in-focus MBAS-WFFM image, (c) a bright-field image, (b1) a magnified MBAS-WFFM image in a selected ROI area. Yellow arrows in (c) and (b) mark the identical blood vessel. The green boxes represent the same ROI in the WFFM image and the bright-field image.

captured in the full FOV image with a folded zone in the middle (Fig. 4(a)). The magnified image showed densely distributed GC clusters in the palpebral conjunctiva. Right after the alkali burn, the WFFM images in both the large and small FOVs showed no GCs at all but homogeneous fluorescence in the conjunctiva. The homogeneous fluorescence could be due to the damage of conjunctival epithelium and the penetration of moxifloxacin solution into the conjunctival stroma (Fig. 4(b)). On day 30 post-burn, the WFFM images visualized GCs again, indicating their recovery (Fig. 4(c)). However, GC clusters were small, and GCs were sparsely distributed in the WFFM image on day 30 post-burn compared to the ones before the burn induction. The magnified WFFM image showed the irregular distribution of GCs. GC clusters were small and there were empty spaces with no GCs. These differences in GCs and GC clusters indicated either partial recovery or recovery in progress. A previous alkali burn study showed that GC density in the conjunctiva did not recover to the normal level after severe burn but converged at best [12]. Our results were consistent with the result in the previous report. The changes of GC density in alkali burn mouse models were analyzed quantitatively. A strip of conjunctival region along the eyelid boundary, approximately 300 μm away from the boundary and approximately 300 μm wide, was selected as the ROI. The ROI was marked by red dashed lines in Fig. 4. GC density was analyzed in the ROI by calculating the mean and standard deviation. GC densities were

Biomedical Optics EXPRESS

approximately 2200 ± 200 cells/mm^2 and 1000 ± 200 cells/mm^2 before the burn and on day 30 post-burn, respectively.

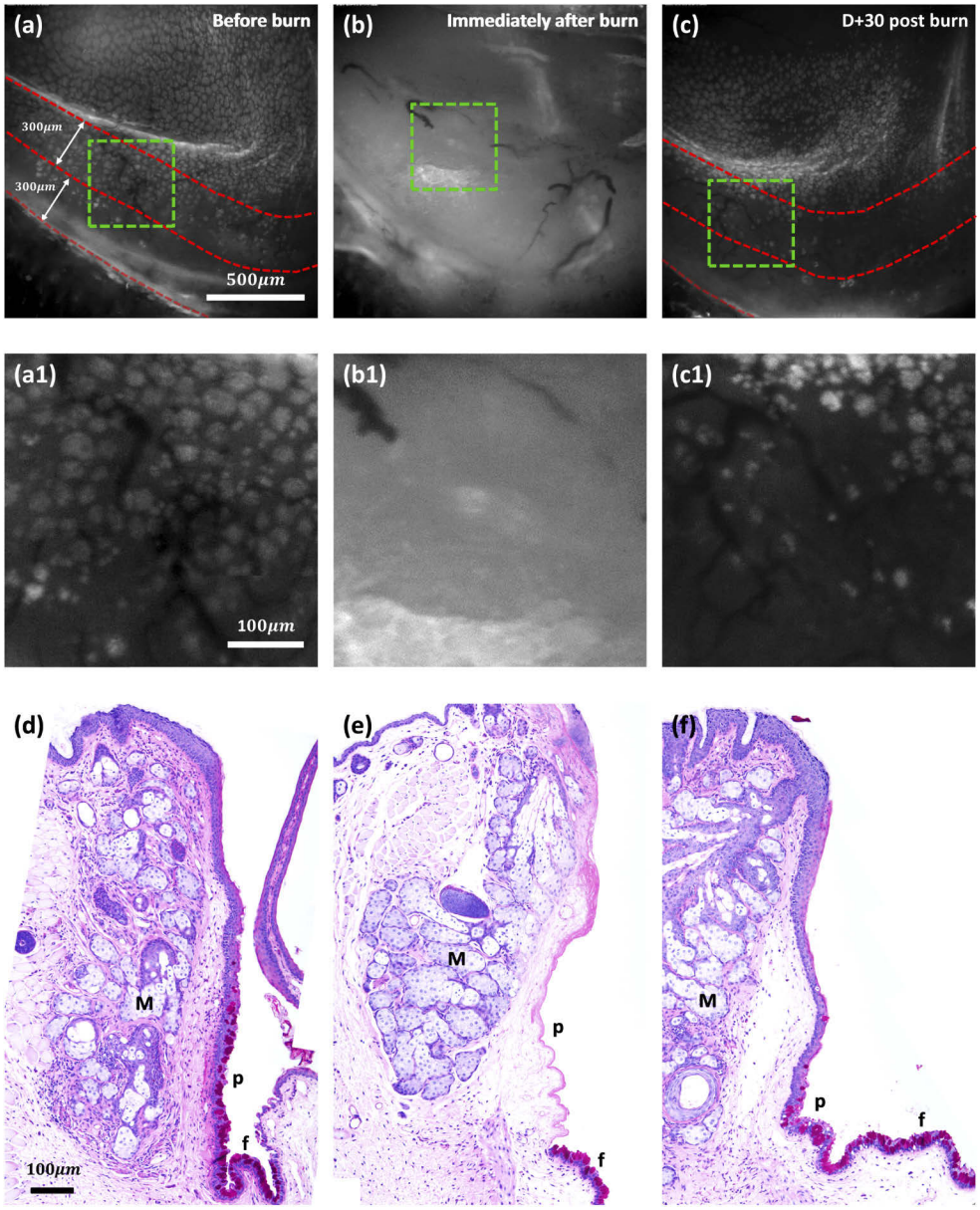

Fig. 4. WFFM and PAS histology images of the conjunctiva in alkali burn mouse models. (a-c): WFFM images before burn (a), immediately after burn (b), and 30 days after burn induction (c). (a1-c1): magnified WFFM images showing the change of individual GC clusters. (d-f): PAS histology images before burn (d), immediately after burn (e), and 30 days after burn induction (f). The area between red dashed lines are selected for GC density calculation. M, Meibomian gland; p, palpebral conjunctiva; f, fornix.

For the confirmation of the GC changes detected by MBAS-WFFM, the conjunctiva tissues were processed for histology with PAS staining. Histology results showed different GC distributions

Biomedical Optics EXPRESS

before, right after, and 30 days after the burn induction. The histological image before the burn showed dense GCs and epithelial cells in the palpebral conjunctiva. The one immediately after burn showed neither GCs nor epithelial cells in the palpebral conjunctiva. The one on day 30 post-burn showed GCs and epithelial cells in the conjunctiva, indicating their recovery. The histology results were consistent with the *in vivo* MBAS-WFFM imaging results.

4. Discussion and conclusion

A new non-invasive high-speed high-contrast GC imaging method was developed. MBAS-WFFM was based on wide-field fluorescence imaging for high-speed imaging and could produce high-contrast images of GCs with moxifloxacin labeling. MBAS-WFFM translated the focal plane axially with the continuous imaging to capture GCs on the tilted surface in focus. The acquired WFFM images with the axial translation were merged to a single all-in-focus image. The generated all-in-focus image showed GCs in high contrasts and enough resolutions. MBAS-WFFM was compared with TPM in the imaging of normal mouse conjunctiva, *ex vivo* (Supplement 1). MBAS-WFFM visualized GCs on the surface of the conjunctiva similarly to TPM, although the MBAS-WFFM image had the higher background than the TPM image. An image analysis algorithm was developed for the quantitative analysis of GC density. The new GC imaging method and image analysis algorithm were characterized in the *in vivo* imaging of normal mouse conjunctivas and then were applied to alkali burn mouse models. The damage of GCs by alkali burn and the recovery afterward were observed and analyzed quantitatively by measuring GC densities.

MBAS-WFFM has several advantages over 3D fluorescence microscopy such as confocal microscopy in the imaging speed, imaging FOV, and system complexity. MBAS-WFFM could image GCs much faster than confocal microscopy by imaging frame by frame rather than pixel by pixel. The imaging speed of MBAS-WFFM was 30 fps for individual WFFM images, limited by the current camera speed. The typical acquisition time of a single stack of axially swept WFFM images was 2 s in total: 1 s for the acquisition of approximately 30 frames during the axial sweeping, and another 1 s for the acceleration of the translational stage. Although MBAS-WFFM had the similar imaging speed to high-speed confocal microscopy, the effective imaging speed of MBAS-WFFM was much higher than confocal microscopy by imaging in the larger FOV. The FOV of MBAS-WFFM was 1.6 mm $\times$ 1.6 mm by using a low magnification objective lens and was approximately 4 times larger in each side than the FOV of confocal microscopy. An air objective lens with a long working distance was used in the current system, and high-contrast GC images could be obtained without physical contact. On the other hand, confocal microscopy typically uses an immersion objective lens for high-resolution 3D imaging, and the physical contact between the objective lens and the sample via immersion media is unavoidable and inconvenient. MBAS-WFFM had much the simpler system configuration and imaging protocol than confocal microscopy.

The GC density analysis algorithm was based on intensity analysis. In the process of converting GC intensity images to binary images via thresholding, some single GC images, which were dim and small, were not counted as valid pixels. Therefore, the current algorithm tended to under-estimate the GC density. More sophisticated analysis algorithms using information of morphology as well as intensity need to be developed for the correct assessment of GC density. MBAS-WFFM used a 405 nm excitation light for exciting moxifloxacin. Because the wavelength of excitation light was in short visible, too much exposure might cause photo-toxicity to the sample. The damage threshold with 405 nm wavelength light was reported to be approximately 54 J/cm^2 [24]. The excitation energy, used in the MBAS-WFFM imaging of mouse conjunctiva, was approximately 0.2 J/cm^2, which was approximately 100 times lower than the damage threshold. Therefore, MBAS-WFFM imaging of GCs should be safe. We also found no sign of damage in the mouse eyes in the conjunctiva, cornea, and other regions during and after the imaging. Rigorous

Biomedical Optics EXPRESS

studies about the effects of excitation light on GCs including molecular analysis are needed for the future application to human subjects. MBAS-WFFM was able to detect the change of GC density in between the control mice (before-burn) and alkali burn mice. Although the alkali burn mouse models were used in the study, the new method provides quantitative information of GCs and it could be possible to detect minute changes of GCs. A study using other disease models could be conducted in the future.

In this study, hairless mice (SKH1-Hrhr) were used for the *in vivo* imaging rather than classical strain mice simply for the convenience of mouse handling. During the *in vivo* imaging of conjunctival GCs, the eyelid of mouse was rolled open and fixed with taping. The skin of hairless mouse was easy to hold with taping. C57BL/6 mice were imaged (data not shown), and the GC images were similar to those of hairless mice. Mice of classical strains could be used in the future study with the improvement of mouse handling skills. We did not do the contralateral investigation in this study. Alkali burn was induced in one eyes of the mice so that the other normal eyes could be imaged for the contralateral investigation. However, we noticed that the normal eyes were not kept closed during the imaging of damaged eyes. We were afraid that the normal eyes could be affected by the imaging, although we kept them moisturized with saline. For the contralateral study, the normal eyes need to be well protected by using gels and the protection protocol needs to be confirmed.

The current MBAS-WFFM system was sub-optimal and there were rooms for improvement. The current imaging protocol was not optimized so that the imaging time including the preparation time was quite long. In the current imaging procedure, the imaging plane was manually positioned at the deepest location of the conjunctiva initially and was translated outward during the continuous WFFM imaging. These steps could be automated by implementing an auto-focusing mechanism. The auto-focusing mechanism could quickly set the initial position of the objective lens without manual adjustment. The image reconstruction process took approximately 5s in MATLAB. The implementation of algorithm in a low-level language such as C/C++ would reduce the computation time down to less than 1s. The shallow DOF limitation of the current system could be relieved by adapting extended DOF (EDOF) methods based on the axicon lens or phase plate [30,31]. This will reduce the number of images to be acquired, the effect of motion artifacts such as breathing motion, and the amount of excitation light exposure. MBAS-WFFM can be developed for the rapid and non-invasive GC examination in the clinic in the future. However, the current system is in infancy, and more development and verification are needed for the translation to the eye clinic. The next step would be the verification of MBAS-WFFM in both large animal models such as rabbits and the animal models of specific diseases associated with GC dysfunction including dry eye disease.

In conclusion, MBAS-WFFM and image processing algorithms were developed for the high-speed high-contrast and non-invasive imaging of GCs in the conjunctiva. The performance of MBAS-WFFM was demonstrated in both the normal and alkali burn mouse models, *in vivo*. The imaging results was consistent with PAS histology. GC density was analyzed from the high-contrast MBAS-WFFM images. The study showed the high potential of MBAS-WFFM as a non-invasive GC examination method in the future.

Funding

Ministry of Science and ICT, South Korea (2020-0-00989, NRF-2020R1A2C3009309); Ministry of Science, ICT & Future Planning of the Korean Government (NRF-2017M3C7A 1044964).

Acknowledgments

This study was supported in part by the Institute of Information & Communications Technology Planning & Evaluation (IITP) grant (No.2020-0-00989) funded by the Korea government (MSIT), Brain Research Program through the National Research Foundation of Korea (NRF)

Biomedical Optics EXPRESS

(NRF-2017M3C7A 1044964) funded by the Ministry of Science, ICT & Future Planning of the Korean Government, and the National Research Foundation of Korea (NRF) grant (NRF-2020R1A2C3009309) funded by the Korea government (MSIT).

Disclosures

SK, MJK, and KHK are authors of a patent filed for moxifloxacin-based imaging of goblet cells.

See Supplement 1 for supporting content.

References

1. J. C. Moore and J. M. Tiffany, "Human ocular mucus. Origins and preliminary characterisation," Exp. Eye Res. **29**(3), 291–301 (1979).
2. C. Baudouin, M. Rolando, J. M. Benitez Del Castillo, E. M. Messmer, F. C. Figueiredo, M. Irkec, G. Van Setten, and M. Labetoulle, "Reconsidering the central role of mucins in dry eye and ocular surface diseases," Prog. Retinal Eye Res. **71**, 68–87 (2019).
3. R. H. Rengstorff, "The precorneal tear film: breakup time and location in normal subjects," Optom. Vis. Sci. **51**(10), 765–769 (1974).
4. S. C. Tseng, L. W. Hirst, A. E. Maumenee, K. R. Kenyon, T. T. Sun, and W. R. Green, "Possible mechanisms for the loss of goblet cells in mucin-deficient disorders," Ophthalmology **91**(6), 545–552 (1984).
5. T. H. Wakamatsu, E. A. Sato, Y. Matsumoto, O. M. Ibrahim, M. Dogru, M. Kaido, R. Ishida, and K. Tsubota, "Conjunctival in vivo confocal scanning laser microscopy in patients with Sjogren syndrome," Invest. Ophthalmol. Visual Sci. **51**(1), 144–150 (2010).
6. S. C. Pflugfelder, S. C. Tseng, K. Yoshino, D. Monroy, C. Felix, and B. L. Reis, "Correlation of goblet cell density and mucosal epithelial membrane mucin expression with rose bengal staining in patients with ocular irritation," Ophthalmology **104**(2), 223–235 (1997).
7. J. D. Nelson and J. C. Wright, "Conjunctival goblet cell densities in ocular surface disease," Arch. Ophthalmol. **102**(7), 1049–1051 (1984).
8. R. A. Ralph, "Conjunctival goblet cell density in normal subjects and in dry eye syndromes," Invest. Ophthalmol. Visual Sci. **14**(4), 299–302 (1975).
9. C. K. Marko, B. B. Menon, G. Chen, J. A. Whitsett, H. Clevers, and I. K. Gipson, "Spdef null mice lack conjunctival goblet cells and provide a model of dry eye," Am. J. Pathol. **183**(1), 35–48 (2013).
10. Q. H. Le, W. T. Wang, J. X. Hong, X. H. Sun, T. Y. Zheng, W. Q. Zhu, and J. J. Xu, "An in vivo confocal microscopy and impression cytology analysis of goblet cells in patients with chemical burns," Invest. Ophthalmol. Visual Sci. **51**(3), 1397–1400 (2010).
11. A. R. Kethiri, E. Raju, K. K. Bokara, D. K. Mishra, S. Basu, C. M. Rao, V. S. Sangwan, and V. Singh, "Inflammation, vascularization and goblet cell differences in LSCD: Validating animal models of corneal alkali burns," Exp. Eye Res. **185**, 107665 (2019).
12. J. Friend, T. Kiorpes, and R. A. Thoft, "Conjunctival goblet cell frequency after alkali injury is not accurately reflected by aqueous tear mucin content," Invest. Ophthalmol. Visual Sci. **24**(5), 612–618 (1983).
13. S. C. Tseng, "Staging of conjunctival squamous metaplasia by impression cytology," Ophthalmology **92**(6), 728–733 (1985).
14. L. H. Colorado, Y. Alzahrani, N. Pritchard, and N. Efron, "Assessment of conjunctival goblet cell density using laser scanning confocal microscopy versus impression cytology," Cont. Lens Anterior Eye **39**(3), 221–226 (2016).
15. M. Calonge, Y. Diebold, V. Saez, A. E. de Salamanca, C. Garcia-Vazquez, R. M. Corrales, and J. M. Herreras, "Impression cytology of the ocular surface: a review," Exp. Eye Res. **78**(3), 457–472 (2004).
16. P. Kumar, R. Bhargava, M. Kumar, S. Ranjan, M. Kumar, and P. Verma, "The correlation of routine tear function tests and conjunctival impression cytology in dry eye syndrome," Korean J. Ophthalmol. **28**(2), 122–129 (2014).
17. D. D. Altinors, S. Bozbeyoglu, G. Karabay, and Y. A. Akova, "Evaluation of ocular surface changes in a rabbit dry eye model using a modified impression cytology technique," Curr. Eye Res. **32**(4), 301–307 (2007).
18. M. J. Doughty, "On the Variability in Goblet Cell Density in Human Bulbar Conjunctival Samples Collected by Impression Cytology with Millicell-CM Biopore Membrane Units," Curr. Eye Res. **41**(11), 1393–1399 (2016).
19. E. M. Messmer, M. J. Mackert, D. M. Zapp, and A. Kampik, "In vivo confocal microscopy of normal conjunctiva and conjunctivitis," Cornea **25**(7), 781–788 (2006).
20. M. Rajadhyaksha, A. Marghoob, A. Rossi, A. C. Halpern, and K. S. Nehal, "Reflectance confocal microscopy of skin in vivo: From bench to bedside," Lasers Surg. Med. **49**(1), 7–19 (2017).
21. E. Cinotti, A. Singer, B. Labeille, D. Grivet, P. Rubegni, C. Douchet, F. Cambazard, G. Thuret, P. Gain, and J. L. Perrot, "Handheld In Vivo Reflectance Confocal Microscopy for the Diagnosis of Eyelid Margin and Conjunctival Tumors," JAMA Ophthalmol. **135**(8), 845–851 (2017).

Biomedical Optics EXPRESS

22. T. Wang, W. H. Jang, S. Lee, C. J. Yoon, J. H. Lee, B. Kim, S. Hwang, C. P. Hong, Y. Yoon, G. Lee, V. H. Le, S. Bok, G. O. Ahn, J. Lee, Y. S. Gho, E. Chung, S. Kim, M. H. Jang, S. J. Myung, M. J. Kim, P. T. C. So, and K. H. Kim, "Moxifloxacin: Clinically compatible contrast agent for multiphoton imaging," Sci. Rep. **6**(1), 27142 (2016).
23. S. Kim, S. Lee, H. Chang, M. Kim, M. J. Kim, and K. H. Kim, "In vivo fluorescence imaging of conjunctival goblet cells," Sci. Rep. **9**(1), 15457 (2019).
24. P. Ramakrishnan, M. Maclean, S. J. MacGregor, J. G. Anderson, and M. H. Grant, "Cytotoxic responses to 405 nm light exposure in mammalian and bacterial cells: Involvement of reactive oxygen species," Toxicol. In Vitro **33**, 54–62 (2016).
25. C. Tomasi and R. Manduchi, "Bilateral filtering for gray and color images," in *Sixth International Conference on Computer Vision* (1998), pp. 839–846.
26. K. Zuiderveld, "Contrast limited adaptive histogram equalization," in *Graphics gems IV* (1994), pp. 474–485.
27. S. Gupta and S. G. Mazumdar, "Sobel edge detection algorithm," Int. J. Comput. Sci. Manag. Res. **2**(2), 1578–1583 (2013).
28. M. J. Doughty and J. P. Bergmanson, "Heterogeneity in the ultrastructure of the mucous (goblet) cells of the rabbit palpebral conjunctiva," Clin. Exp. Optom. **87**(6), 377–385 (2004).
29. A. J. W. Huang, S. C. G. Tseng, and K. R. Kenyon, "Morphogenesis of Rat Conjunctival Goblet Cells," Invest. Ophthalmol. Visual Sci. **29**(6), 969–975 (1988).
30. Z. S. Zhai, S. T. Ding, Q. H. Lv, X. Z. Wang, and Y. N. Zhong, "Extended depth of field through an axicon," J. Mod. Opt. **56**(11), 1304–1308 (2009).
31. H. Zhao and Y. C. Li, "Optimized sinusoidal phase mask to extend the depth of field of an incoherent imaging system," Opt. Lett. **35**(2), 267–269 (2010).